 CMES, vol.15, no.3, pp.165-177, 2006

Efficient Green's Function Modeling of Line and Surface Defects in Multilayered Anisotropic Elastic and Piezoelectric Materials[1]

B. Yang[2] and V. K. Tewary[3]

Abstract: Green's function (GF) modeling of defects may take effect only if the GF as well as its various integrals over a line, a surface and/or a volume can be efficiently evaluated. The GF is needed in modeling a point defect, while integrals are needed in modeling line, surface and volumetric defects. In a matrix of multilayered, generally anisotropic and linearly elastic and piezoelectric materials, the GF has been derived by applying 2D Fourier transforms and the Stroh formalism. Its use involves another two dimensions of integration in the Fourier inverse transform. A semi-analytical scheme has been developed previously for efficient evaluation of the GF. In this paper, an efficient scheme for evaluation of the line and surface integrals of the GF is presented. These integrals are obtained by carrying out the integration over the physical domain analytically and then over the transform domain numerically. The efficiency is thus comparable to that in the evaluation of the GF. The high efficiency in the evaluation of the surface integral is of particular value to the modeling of dislocations due to the lack of a line-defect treatment of this group of defects (originally, of uniform planar distribution of force dipoles) in a multilayered heterogeneous matrix. Numerical examples of nitride semiconductors with strong piezoelectric effect are presented to demonstrate the efficiency and accuracy of the present scheme.

keyword: Anisotropy, Defects, Dislocations, Elasticity, Fourier transforms, Green's function, Multilayers, Piezoelectricity, Semiconductors, Steps, Stroh formalism.

1 Introduction

Defects are of great importance in materials science and engineering as well as in applied mechanics. They may occur at a "point" (such as vacancies and interstitials at the lattice level), along a line (such as surface and interfacial steps), over a surface (such as dislocations, disclinations, and cracks) and over a finite volume (such as quantum dots, and reinforcing particles in composites) (Eshelby, 1956; Mura, 1982; Hirth and Lothe, 1991; Nemat-Nasser and Hori, 1999). When they are modeled in a continuum matrix as concentrated sources of force, dipole, or multipole of any higher order, the stress and strain fields are singular or nearly singular in their vicinity. Obviously such rapidly varying fields would be troublesome to a completely numerical scheme and hence require analytical treatment (Weygand *et al*., 2002; O'Day and Curtin, 2004). It has been well known that a point-source Green's function (GF) is ideal for modeling defects. It can be directly applied to model point defects. To model line, surface and volumetric defects, it then needs to be integrated over the corresponding defect space. The GF method has long been recognized for high efficiency and high accuracy in modeling defects in an infinite, homogeneous, isotropic matrix, where the GF, namely, the Kelvin fundamental solution, is available in an explicit analytical form (Love, 1944; Mura, 1982).

Within the theory of generally anisotropic linear elasticity and piezoelectricity, the GFs of infinite-space, half-space, bimaterials, trimaterials and multilayers have been derived in a series of papers in recent years (Wang, 1997; Pan and Tonon, 2000; Pan and Yuan, 2000a, b; Yang and Pan, 2002a, b; Pan and Yang, 2003; Yuan et al., 2003; Yang et al., 2004). The infinite-space GF was given in an analytical form. However, because it involves numerical solution of an eigen-equation, its evaluation is less efficient than that of the explicit Kelvin solution in an infinite isotropic matrix. The other GFs of heterogeneous systems were derived by applying two-dimensional (2D) Fourier transforms and the Stroh formalism (Stroh, 1958;

[1] Publication of the National Institute of Standards and Technology, an agency of the US Government; not subject to copyright.

[2] Correspondence author. Department of Mechanical and Aerospace Engineering, Florida Institute of Technology, Melbourne, FL 32901. Email: boyang@fit.edu.

[3] Materials Reliability Division, National Institute of Standards and Technology, Boulder, CO 80305

Ting, 1996). The bimaterial GF, including the half-space GF as a special case, was derived as a 1D integral by analytically integrating over the radial axis in the inverse transform. The trimaterial GF was obtained as an infinite series of 1D integrals, equivalent to the series solution by an image method (Yu and Sanday, 1993). When both the field and source points are located on the same interface, special care must be taken to deal with the finite-part integrals. Finally, the multilayer GF was divided in two parts, special (seed) and general (complimentary). The special part is taken to be one of the above GFs, which can be evaluated either analytically or numerically in a 1D integral. The general part inevitably involves a 2D numerical integral in the Fourier inverse transform. There are subtle issues in carrying out the inverse transform efficiently, which however are not discussed here. Rather we would like to point out that when these GFs are applied to solve a defect problem that requires integration over a physical space, the problem size would soon reach the limit set by currently available computer power. In this paper, an efficient scheme is developed to evaluate the line and surface integrals of the GF in multilayered elastic and piezoelectric materials. The evaluation is accomplished by carrying out the integration first over the physical domain analytically and then over the transform domain numerically. The efficiency attained in this way is nearly as high as that in the evaluation of the GF (Yang and Pan, 2002b). Such high efficiency would be critical to a simulation of a large system of defects including steps and dislocations in the heterogeneous materials.

The present work was motivated by recent great interest in studying steps and dislocations in thin films and multilayers and hence demand for their efficient modeling and simulation (Liu *et al*., 1997; Heying *et al*., 1999; Han and Ghoniem, 2005). Thin films and multilayers are often found as the base structure in advanced electronic devices as well as in protective coatings and thermal barriers. The presence of surfaces and interfaces poses a significant challenge to the computational modeling of defects. Steps may be buried at an interface or exposed at a free surface. For instance, an interfacial step may emerge as a dislocation penetrating an interface. In turn, a surface step may form as a dislocation terminating at a surface, through surface instability over a strained substrate, and during incomplete deposition of a monolayer in epitaxy. The continuum modeling of steps as line defects is straightforward. Its nature, i.e., order and intensity of singularity, whether a force, dipole, or multipole of any higher order, may be determined through atomistic simulations and first-principles calculations (Balamane *et al*., 1992; Van de Walle *et al*., 1998).

In its nature, a dislocation was initially modeled as a surface defect of uniform displacement discontinuity (Mura, 1963, 1982). The induced displacement and stress fields can be conveniently expressed as a surface integral with the GF of the matrix as kernel over the dislocation slip plane. If the matrix is homogeneous and infinite and thus holds complete translational symmetry, the surface integral for evaluation of stress due to a surface dislocation can be reduced to a line integral with its source distributed along the dislocation edge (Mura, 1963, 1982). The dislocation is consequently regarded as a linear "line defect". However, it must be remarked that such a line-defect treatment for evaluation of displacement due to a dislocation has not been derived even in the simplest case of an infinite, homogeneous matrix. The line-defect treatment of dislocations for evaluation of stress has been extended to the case of a homogeneous traction-free half-space (Gosling and Willis, 1996). The image forces of a dislocation in the presence of a free surface can be accounted for by compensating the traction at the surface caused by the dislocation in an infinite homogeneous space. That is, a boundary value problem is solved, in which the traction-free surface condition is imposed, and in which the Mura's fundamental (referring to an infinite space) solution of stress due to an infinitesimal "line-dislocation" segment is taken as the special (seed) solution. This is feasible because the fundamental solution for displacement, which is unavailable as remarked above, is not required in the imposition of traction-free surface condition in this case. For the same reason, the line-defect treatment of dislocations can be extended to a free-standing film for evaluation of stress. Arias and Lund (1999) proposed a formulation for a line-integral treatment of dislocation in finite samples. They presented as examples the traction-free half-space and the free-standing plate, the same two cases discussed above. It is unclear how their formulation could be applied to other cases where the (unavailable) fundamental solution for displacement is required to enforce boundary conditions and/or interfacial continuity conditions.

Ghoniem and Han (2005) developed a line-integral formulation of dislocation in multilayered materials by solving the boundary-value problem of a "line-dislocation"

segment, similarly to solving the boundary-value problem of a point force by Yang and Pan (2002b) and Yuan et al. (2003). Unlike the aforementioned cases of a traction-free half-space and a free-standing film, this case requires the fundamental solution for displacement due to a "line-dislocation" segment in order to impose the complete continuity condition of both displacement and traction across an interface. Ghoniem and Han proposed to bypass this requirement by imposing the continuity condition of displacement gradient along the interfaces (Hill, 1961). However, their expression for displacement gradient (equation (2) in the paper) lacks a term of displacement discontinuity across the dislocation slip plane, given in the Dirac delta function, according to Mura (1982) (page 39). This invalidates their formulation, as may be evidenced by an obvious discrepancy between their solutions (Figure 2 in the paper) by the line-integral method and the original surface-integral method (Han and Ghoniem, 2005). A line-integral expression for displacement gradient due to a dislocation would be available only if the Dirac delta function can be dissolved into a line integral along the dislocation edge as well, which is unknown yet and seems difficult, if not impossible.

The present paper is organized as follows. In Section 2, the theory of anisotropic and linear piezoelectricity is summarized, including elasticity and electrostatics as special cases. Within the framework, various point, line and surface defects are modeled by using GFs. In Section 3, the GFs of a point source (i.e., force or charge) in multilayered elastic and piezoelectric materials are summarized. Based on the characteristics of the GF, a scheme is proposed for efficient evaluation of their line and surface integrals in the physical space, which are required in the modeling of various line and surface defects. In Section 4, numerical examples of dislocations in nitride semiconductors with strong piezoelectric effect are presented to demonstrate the efficiency and accuracy of the present scheme. The solutions due to the elastic and piezoelectric models are compared. In Section 5, conclusions are drawn.

2 Green's Function Method of Defects

In this section, the general formulation of defects in multilayered piezoelectric materials is described. Since the short-hand notation of Barnett and Lothe (1975) is adopted, it is symbolically identical to the elastic case.

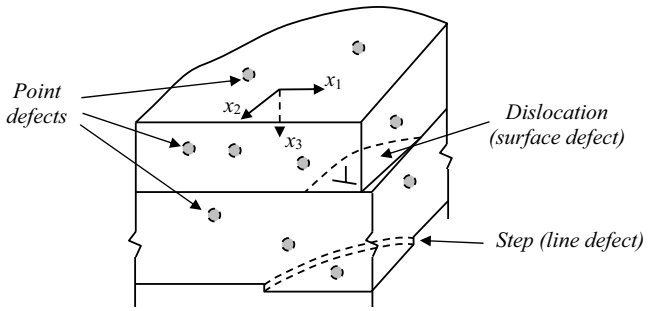

Figure 1 : A multilayered matrix embedded with various point, line and surface defects.

They are only different in the range of indices in certain quantities. In the other words, the formulation of piezoelectricity includes elasticity and electrostatics as special cases. Let us consider a semi-infinite multilayered matrix consisting of multiple planar layers of generally different homogeneous, anisotropic and linearly piezoelectric materials, as schematically shown in Fig. 1. The top surface is free of traction. The interfaces are perfectly bonded. There may exist various point, line and surface defects embedded in or attached to the matrix. The global Cartesian coordinate system (x_1, x_2, x_3) is defined such that the $x_1 - x_2$ plane lies on the top surface and the matrix occupies $x_3 \geq 0$.

The mechanical and electrical equilibrium equations are given by

$$\sigma_{ji,j} + f_i = 0, \quad D_{i,i} - q = 0, \tag{1}$$

where σ_{ji} is the stress component, D_i is the electric displacement component, f_i is the body force component, and q is the electrical charge. The comma in the subscripts indicates partial differentiation with respect to the coordinate that follows. Repeated subscript indices imply the conventional Einstein summation over their ranges.

The constitutive laws for each homogeneous layer are given by

$$\sigma_{ji} = C_{jilm}\gamma_{lm} - e_{kji}E_k, \quad D_i = e_{ijk}\gamma_{jk} + \varepsilon_{ij}E_j, \tag{2}$$

where $g\gamma_{lm}$ is the infinitesimal strain component, E_k is the electric field component, and C_{jilm}, e_{kji}, and ε_{ij} are respectively components of the elastic stiffness, piezoelectric coefficient, and dielectric constant tensors. The strain

and electric field are respectively related to the elastic displacement $\boldsymbol{u}$ and the electric potential ϕ by

$$\gamma_{ij} = \tfrac{1}{2}(u_{i,j} + u_{j,i}), \quad E_i = -\phi_{,i}. \tag{3}$$

For convenience in analyzing the anisotropic piezoelectric problem, the notation of Barnett and Lothe (1975) is adopted in the present work. This notation introduces the extended displacement, strain, stress and materials constants as follows:

$$u_I = \begin{cases} u_i & I(=i) = 1,2,3 \\ \phi & I = 4 \end{cases}, \tag{4}$$

$$\gamma_{Ij} = \begin{cases} \gamma_{ij} & I(=i) = 1,2,3 \\ -E_j & I = 4 \end{cases}, \tag{5}$$

$$\sigma_{iJ} = \begin{cases} \sigma_{ij} & J(=j) = 1,2,3 \\ D_i & J = 4 \end{cases}, \tag{6}$$

$$C_{iJKl} = \begin{cases} C_{ijkl} & J(=j), K(=k) = 1,2,3 \\ e_{lij} & J(=j) = 1,2,3;\ K = 4 \\ e_{ikl} & J = 4;\ K(=k) = 1,2,3 \\ -\varepsilon_{il} & J = K = 4 \end{cases}, \tag{7}$$

where the upper-case subscripts range from 1 to 4, and the lower-case subscripts from 1 to 3.

In terms of this short-hand notation, the equilibrium equations in Eq. (1) can be unified as

$$\sigma_{jI,j} + f_I = 0, \tag{8}$$

with

$$f_I = \begin{cases} f_i & I(=i) = 1,2,3 \\ -q & I = 4 \end{cases}. \tag{9}$$

Similarly, the constitutive laws in Eq. (2) are recast into

$$\sigma_{iJ} = C_{iJKl}\gamma_{Kl}. \tag{10}$$

Substituting Eq. (10) in Eq. (8) and realizing the symmetry in the strain tensor (before extension), the equilibrium equation of displacement is given by

$$(C_{jIKl}u_{K,l})_{,j} + f_I = 0. \tag{11}$$

Defects of any kind may be originally modeled as a system of concentrated forces and charges, or say, concentrated forces in the extended notation. The forces are taken to be the Kanzaki force, including the unrelaxed physical force derived by differentiating the interatomic potential with respect to atomic position about a ground state plus a term due to the change of interatomic force constant and associated lattice distortion (Kanzaki, 1957; Tewary, 1973, 2004). Thus, the GF of the multilayered matrix in the absence of any defects can be applied to derive the field due to these forces by the principle of superposition as

$$u_P(\mathbf{X}) = \sum_n G_{PI}(\mathbf{X},\mathbf{x}^{(n)})F_I^{0(n)}, \tag{12}$$

where $\boldsymbol{x}^{(n)}$ is the location of the nth individual force $\boldsymbol{F}^{0(n)}$, and $G_{PI}(\mathbf{X},\mathbf{x})$ is the GF of the Ith displacement component at field point $\boldsymbol{x}$ due to a unit point force applied along the Pth direction if $P \leq 3$ and due to a unit point charge if $P = 4$ at source point $\boldsymbol{X}$. Throughout the text, letters $i$through$n$ are used to indicate the association of a subscript index with field point $\boldsymbol{x}$, while the other letters are associated with source point $\boldsymbol{X}$ unless indicated otherwise.

The above forces modeling defects are grouped in small volumetric, surface and line elements according to their spatial distribution and location. Within each group, the GF $G_{PI}(\mathbf{X},\mathbf{x})$ associated with an individual force in Eq. (12) is expanded in the Taylor series around the average site $\boldsymbol{x}^{(group)}$. By rearranging, Eq. (12) may be recast into

$$\begin{aligned} u_P(\mathbf{X}) = \sum_{group} \Big\{ & G_{PI}(\mathbf{X},\mathbf{x}^{(group)})F_I^{0(group)} \\ & + G_{PI,j}(\mathbf{X},\mathbf{x}^{(group)})M_{jI}^{0(group)} + \\ & + G_{PI,jk}(\mathbf{X},\mathbf{x}^{(group)})T_{jkI}^{0(group)} \\ & + \sum_n o((\mathbf{x}^{(n)} - \mathbf{x}^{(group)})^3) \Big\}, \end{aligned} \tag{13}$$

with

$$F_I^{0(group)} = \sum_n F_I^{0(n)}, \tag{14}$$

$$M_{jI}^{0(group)} = \sum_n (x_j^{(n)} - x_j^{(group)})F_I^{0(n)}, \tag{15}$$

$$T_{jkI}^{0(group)} = \sum_n (x_j^{(n)} - x_j^{(group)})(x_k^{(n)} - x_k^{(group)})F_I^{0(n)}, \tag{16}$$

where $F_I^{0(group)}$, $M_{jI}^{0(group)}$, and $T_{jkI}^{0(group)}$ are called the net force, dipole, and tripole tensors, and the summations in these expressions are within each group. If necessary,

more terms of multipole tensor at any higher order can be added to characterize a defect.

Point and Line Defects. Common point defects including vacancies, substitutions, interstitials and surface adatoms are normally characterized as a dipole. They introduce no net force to a matrix. Rarely a surface point defect may behave like a tripole (Swamy *et. al*, 1999). An interfacial step may be caused by the penetration of a dislocation through an interface. If the host materials contain uneven residual stresses, net force would appear along the step. The force density may be roughly estimated as the product of step height and difference of residual stresses across the interface. An interfacial step may also behave like a dipole if the residual stresses are the same across the interface, including the case that the host materials are free of residual stress. In contrast, a surface step may be formed in several ways, including termination of a dislocation at a surface, surface instability over a strained substrate, and incomplete deposition of a monolayer in epitaxy. Because severe atomic rearrangement is likely to occur due to the high mobility of atoms at a surface, a surface step would exhibit at most the behavior of a dipole. The displacement fields due to these point and line defects are given by

$$u_P(\mathbf{X}) = \sum_{PD} G_{PI,j}(\mathbf{X},\mathbf{x}^{(PD)}) M_{jI}^{0(PD)} \quad \text{for point defects,} \tag{17}$$

$$u_P(\mathbf{X}) = \sum_{LD} \int_{l^{(LD)}} [G_{PI}(\mathbf{X},\mathbf{x}) F_I^{0(LD)}(\mathbf{x}) + G_{PI,j}(\mathbf{X},\mathbf{x}) M_{jI}^{0(LD)}(\mathbf{x})] dl(\mathbf{x}) \quad \text{for line defects,} \tag{18}$$

where $M^{0(PD)}$ is the dipole tensor of a point defect (*PD*), and $\boldsymbol{F}^{0(LD)}$ and $M^{0(LD)}$ are the densities of force and dipole tensors (per unit length) along a line defect (*LD*).

Surface Defects. A dislocation is a surface defect with atoms on one side of the surface sliding relative to those on the other side. The relative displacement is uniform except near the edge where severe (nonlinear) lattice distortion may occur. Solution to the entire force system in this case would be difficult due to the huge defect space. Fortunately, the portion of lattice undergoing severe (nonlinear) distortion is small compared to the total defect space. Treating a dislocation as a singular surface of uniform displacement discontinuity neglecting the effect of nonlinear core near the edge has been commonly accepted. Within the approach, the Kanzaki force can be easily estimated. It can be originally obtained within the lattice theory, equaled to the force-constant change times the displacement in the defect space along the dislocation slip plane. It would then be turned into the continuum counterpart. This linkage of lattice and continuum length scales in modeling a dislocation is interesting and will be discussed in detail elsewhere. The forces of a dislocation are self-balanced if any net charge is excluded. Their separation normal to the dislocation slip plane produces a surface source of dipole. Thus, the induced displacement field by dislocations is given by

$$u_P(\mathbf{X}) = \sum_{SD} \int_{S^{(SD)}} G_{PI,j}(\mathbf{X},\mathbf{x}) M_{jI}^{0(SD)} dS(\mathbf{x}), \tag{19}$$

with

$$M_{jI}^{0(SD)} = -C_{jIKl} b_K n_l, \tag{20}$$

where $\boldsymbol{n}$ is the outward normal vector on one side of the slip plane, and $\boldsymbol{b}$ is the displacement jump across the slip plane (defined by the displacement on the side where $\boldsymbol{n}$ is defined minus that on the other side), i.e., the Burgers vector. In case that the dislocation lies entirely in an interface of two distinct materials, the elastic stiffness matrix $\boldsymbol{C}$ in Eq. (20) may be taken from either side of the interface. An identical expression should result because the derivative of $\boldsymbol{G}$ being multiplied by $\boldsymbol{C}$ and further by $\boldsymbol{n}$, i.e., the GF of traction, is continuous across the interface. Note that it is unlikely for $\boldsymbol{b}$ (in the extended notation) to contain a nontrivial component of charge, i.e., discontinuity of charge. In contrast, it is likely to have charge and/or charge dipole distributed along the edge of a dislocation (Look and Sizelove, 1999). In this case, the charged dislocation edge can be modeled as a line defect described in Eq. (18).

Upon obtaining the displacement field, the stress field of defects can be easily derived by differentiating the expression with respect to $\boldsymbol{X}$ and applying the constitutive law in Eq. (10). The total displacement and stress fields are obtained by the principle of superposition in the linear case. One may check Mura (1982) for detail. To evaluate these fields, the GF and its line and surface integrals are required. An efficient scheme for evaluation of the GF is available (Yang and Pan, 2002b). In the next section, a scheme is presented for efficient evaluation of its line and surface integrals by taking effect certain features of the GF.

Before closing this section, it may be worthwhile noting that the above continuum model of defects starts with the force, taken to be the Kanzaki force, instead of eigen-strain and/or eigen-stress (Mura, 1982; Nemat-Nasser and Hori, 1999). It is thus closely linked to the lattice theory of defects (Maradudin *et al*., 1971; Tewary, 1973). A linkage like this through forces invariant on both the continuum and lattice scales would readily lay down a foundation for multiscale modeling of defects (Tewary, 2004; Tewary and Read, 2004; Yang and Tewary, 2005).

3 Evaluation of Green's Function Integrals

The point-source GF $\boldsymbol{G}(\boldsymbol{X}, \boldsymbol{x})$ gives the (extended) displacement $\boldsymbol{u}$ at field point $\boldsymbol{x}$ due to a unit point (extended) force $\boldsymbol{f}$ applied at source point $\boldsymbol{X}$ in a matrix. The displacement $\boldsymbol{u}(\boldsymbol{x})$ satisfies equilibrium Eq. (11). Let us apply the following 2D Fourier transform to the first two variables of a field quantity, for instance, $\boldsymbol{u}$, as

$$\tilde{u}_I(y_1, y_2, x_3) = \iint u_I(x_1, x_2, x_3) e^{iy_\alpha x_\alpha} dx_1 dx_2, \qquad (21)$$

where e stands for the *exponential* function, i denotes the unit of imaginary number, $\sqrt{-1}$, and a Greek subscript (α) ranges from 1 to 2. The integral limits are $(-\infty, \infty)$ along both coordinatesx_1 and x_2. Applying the Fourier transform to the governing Eq. (11) yields

$$C_{3IK3}\tilde{u}_{K,33} - i(C_{\alpha IK3} + C_{3IK\alpha}) y_\alpha \tilde{u}_{K,3} - C_{\alpha IK\beta} y_\alpha y_\beta \tilde{u}_K = -f_I e^{iX_\alpha y_\alpha} \delta(x_3 - X_3), \qquad (22)$$

where $\delta(x_3 - X_3)$ is the 1D Dirac delta function.

Solving the above ordinary differential equation yields a general solution of the displacement in the transformed domain, (Ting, 1996)

$$\tilde{\boldsymbol{u}}(y_1, y_2, x_3) = \boldsymbol{a} e^{-ip\eta x_3}, \qquad (23)$$

where η is the norm of (y_1, y_2), and p and $\boldsymbol{a}$ are the eigenvalue and eigenvector of the Stroh's eigen-equation. Taking the derivative of Eq. (23) and applying the constitutive law, Eq. (10), result in the solution of the extended stress in the transformed domain,

$$\tilde{\boldsymbol{t}} = -i\eta \boldsymbol{b} e^{-ip\eta x_3}, \quad \tilde{\boldsymbol{s}} = -i\eta \boldsymbol{c} e^{-ip\eta x_3}, \qquad (24)$$

where $\boldsymbol{t} \equiv (\sigma_{13}, \sigma_{23}, \sigma_{33}, D_3)^T$ and $\boldsymbol{s} \equiv (\sigma_{11}, \sigma_{12}, \sigma_{22}, D_1, D_2)^T$ consist of the out-of-plane and in-plane stress and electric displacement components, and $\boldsymbol{b}$ and $\boldsymbol{c}$ are the eigenvectors corresponding to the vectors $\boldsymbol{t}$ and $\boldsymbol{s}$, and are related to $\boldsymbol{a}$ and p.

There exist eight sets of eigenvalue p_I and associated eigenvectors $\mathbf{a}_I$, $\mathbf{b}_I$ and $\mathbf{c}_I$. They are arranged in the following way:

$$\begin{aligned} &Im\, p_I > 0, \quad p_{I+4} = \overline{p}_I, \quad \boldsymbol{a}_{I+4} = \overline{\boldsymbol{a}}_I, \quad \boldsymbol{b}_{I+4} = \overline{\boldsymbol{b}}_I, \\ &\boldsymbol{c}_{I+4} = \overline{\boldsymbol{c}}_I \quad (I = 1, 2, 3, 4), \\ &\boldsymbol{A} = [\boldsymbol{a}_1, \boldsymbol{a}_2, \boldsymbol{a}_3, \boldsymbol{a}_4], \quad \boldsymbol{B} = [\boldsymbol{b}_1, \boldsymbol{b}_2, \boldsymbol{b}_3, \boldsymbol{b}_4], \\ &\boldsymbol{C} = [\boldsymbol{c}_1, \boldsymbol{c}_2, \boldsymbol{c}_3, \boldsymbol{c}_4], \end{aligned} \qquad (25)$$

where Im stands for the imaginary part, and the over-bar denotes the complex conjugate. Assuming that p_I (I = 1, 2, 3, 4) are distinct, the general solutions are obtained by superposing the eight solutions of Eqs. (23) and (24), as

$$\tilde{\boldsymbol{u}} = i\eta^{-1}\overline{\boldsymbol{A}} \left\langle e^{-i\overline{\mathbf{p}}\eta x_3} \right\rangle \boldsymbol{v} + i\eta^{-1}\boldsymbol{A} \left\langle e^{-i\mathbf{p}\eta x_3} \right\rangle \boldsymbol{w}, \qquad (26)$$

$$\tilde{\boldsymbol{t}} = \overline{\boldsymbol{B}} \left\langle e^{-i\overline{\mathbf{p}}\eta x_3} \right\rangle \boldsymbol{v} + \boldsymbol{B} \left\langle e^{-i\mathbf{p}\eta x_3} \right\rangle \boldsymbol{w},$$

$$\tilde{\boldsymbol{s}} = \overline{\boldsymbol{C}} \left\langle e^{-i\overline{\mathbf{p}}\eta x_3} \right\rangle \boldsymbol{v} + \boldsymbol{C} \left\langle e^{-i\mathbf{p}\eta x_3} \right\rangle \boldsymbol{w}, \qquad (27)$$

where $\boldsymbol{v}(y_1, y_2)$ and $\boldsymbol{w}(y_1, y_2)$ are unknown complex vectors and

$$\left\langle e^{-i\mathbf{p}\eta x_3} \right\rangle = diag[e^{-ip_1\eta x_3}, e^{-ip_2\eta x_3}, e^{-ip_3\eta x_3}, e^{-ip_4\eta x_3}]. \qquad (28)$$

Note that the above matrix $\boldsymbol{C}$ with 5x4 elements is different from the elastic stiffness matrix C_{ijkl} or the extended stiffness matrixC_{iJKl}.

The displacement and stress fields in each layer, for instance, the mth layer, are given by

$$\begin{aligned} \tilde{\boldsymbol{u}}_m(y_1, y_2, x_3) e^{-iy_\alpha X_\alpha} &= \tilde{\boldsymbol{u}}_m^{(s)}(y_1, y_2, x_3) \\ &+ i\eta^{-1}\overline{\boldsymbol{A}}_m \left\langle e^{-i\overline{p}_m \eta (x_3 - h_{m-1})} \right\rangle \boldsymbol{v}_m \\ &+ i\eta^{-1}\boldsymbol{A}_m \left\langle e^{-ip_m \eta (x_3 - h_m)} \right\rangle \boldsymbol{w}_m, \end{aligned} \qquad (29)$$

$$\begin{aligned} \tilde{\boldsymbol{t}}_m(y_1, y_2, x_3) e^{-iy_\alpha X_\alpha} &= \tilde{\boldsymbol{t}}_m^{(s)}(y_1, y_2, x_3) \\ &+ \overline{\boldsymbol{B}}_m \left\langle e^{-i\overline{p}_m \eta (x_3 - h_{m-1})} \right\rangle \boldsymbol{v}_m \\ &+ \boldsymbol{B}_m \left\langle e^{-ip_m \eta (x_3 - h_m)} \right\rangle \boldsymbol{w}_m, \end{aligned} \qquad (30)$$

$$\tilde{\boldsymbol{s}}_m(y_1, y_2, x_3)e^{-iy_\alpha X_\alpha} = \tilde{\boldsymbol{s}}_m^{(s)}(y_1, y_2, x_3) + \overline{\boldsymbol{C}}_m \left\langle e^{-i\overline{p}_m \eta(x_3 - h_{m-1})} \right\rangle \boldsymbol{v}_m + \boldsymbol{C}_m \left\langle e^{-ip_m \eta(x_3 - h_m)} \right\rangle \boldsymbol{w}_m, \quad (31)$$

where v_m and w_m are unknown vectors to be determined from prescribed interfacial and boundary conditions, and $\tilde{\boldsymbol{u}}_m^{(s)}$, $\tilde{\boldsymbol{t}}_m^{(s)}$ and $\tilde{\boldsymbol{s}}_m^{(s)}$ are special solutions. The special solutions are chosen according to the location of $\boldsymbol{f}$ such that the general-part solutions, i.e., unknown vectors $\boldsymbol{v}_m$ and $\boldsymbol{w}_m$, are nonsingular in the physical space and can be evaluated efficiently. One may check our previous publications for tactics to improve the computational efficiency in evaluation of the GF (Yang and Pan, 2002b; Pan and Yang, 2003; Yang et al., 2004).

By imposing the interfacial continuity and surface boundary conditions, a system of algebraic equations can be derived to solve for unknown vectors $\boldsymbol{v}_m$ and $\boldsymbol{w}_m$. Once the transform-domain solution is derived, the physical responses are obtained by applying the Fourier inverse transform, for instance, the displacement u_I, as

$$u_I(x_1, x_2, x_3) = \frac{1}{(2\pi)^2} \iint \tilde{u}_I(y_1, y_2, x_3) e^{-iy_\alpha x_\alpha} dy_1 dy_2, \quad (32)$$

where the integral limits in both coordinates are from $-\infty$ to ∞.

In the earlier modeling of defects in Sec. 2, the integrals of GF along a line and a surface in the physical domain are required, leading to a 3D and even a 4D integral to be evaluated. If it were carried out entirely numerically, the task would be prohibitively large. In the following, a scheme is presented to lighten the computational burden by integrating the GF first over the physical domain analytically and then over the transform domain numerically. This can be done because in the transform domain, the above GFs of displacement and stress as well as their derivatives with respect to $\boldsymbol{X}$ and/or $\boldsymbol{x}$ (not given for brevity) can all be expressed as a sum of terms in the following form, factored by a coefficient independent of $\boldsymbol{x}$,

$$\iint e^{k_i x_i} dy_1 dy_2, \quad (33)$$

where $\boldsymbol{k}$ is a function of y_1 and y_2. Analytical integrals of the transform-domain GF over a straight line and a flat surface are derived, and presented below.

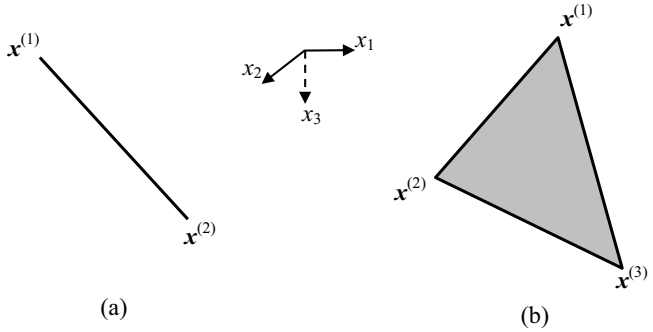

Figure 2 : (a) A straight line element; (b) a flat triangular surface element.

Along a straight line $l(\boldsymbol{x})$ between $\boldsymbol{x}^{(1)}$ and $\boldsymbol{x}^{(2)}$, as shown in Fig. 2(a), the line integral of a term of the GF given in expression (33) can be derived as

$$\iiint e^{k_i x_i} dy_1 dy_2 dl(\mathbf{x}) = L \iint \frac{e^{k_i x_i^{(2)}} - e^{k_i x_i^{(1)}}}{k_i (x_i^{(2)} - x_i^{(1)})} dy_1 dy_2, \quad (34)$$

where L is the length of $l(\boldsymbol{x})$. Since $\boldsymbol{k}$ is distinct for different layers, the line $l(\boldsymbol{x})$ should reside within a single layer in order for the above expression to be valid.

Over a flat, triangular surface element $S(\boldsymbol{x})$ with corners $\boldsymbol{x}^{(1)}$, $\boldsymbol{x}^{(2)}$ and $\boldsymbol{x}^{(3)}$, as shown in Fig. 2(b), the surface integral of a term of the GF given in expression (33) can be derived as

$$\iiint e^{k_i x_i} dy_1 dy_2 dS(\mathbf{x}) = 2A \iint \frac{\left\{ \begin{array}{c} e^{k_i x_i^{(1)}} [k_i (x_i^{(2)} - x_i^{(3)})] + \\ e^{k_i x_i^{(2)}} [k_i (x_i^{(3)} - x_i^{(1)})] + \\ e^{k_i x_i^{(3)}} [k_i (x_i^{(1)} - x_i^{(2)})] \end{array} \right\}}{\left\{ \begin{array}{c} [k_i (x_i^{(2)} - x_i^{(1)})] \times \\ [k_i (x_i^{(3)} - x_i^{(2)})] \times \\ [k_i (x_i^{(1)} - x_i^{(3)})] \end{array} \right\}} dy_1 dy_2, \quad (35)$$

where A is the area of the triangular element. For the same reason as in the case of the line element, surface element $S(\boldsymbol{x})$ should be contained within a single layer.

In solving the general part of GF above, a special solution is required. It may be taken as the infinite-space GF, the bimaterial GF, or a few leading terms of the trimaterial GF. The infinite-space GF may be obtained analytically.

The bimaterial GF and individual terms of the trimaterial GF are given in a 1D integral over the angular axis in the transform domain. Their integration over line and surface elements in the physical space can still be laborious with currently available computer power. Here it is proposed to carry out the physical-domain integration analytically, leaving a 1D integral over the transform-domain angular axis for numerical treatment. This would include the infinite-space GF as a special case of the bimaterials, although it can be evaluated analytically. The present scheme, applied to the infinite-space GF, would result in much higher efficiency in the case of a surface integral and comparable efficiency in the case of a line integral. The 1D integrals of the bimaterial and trimaterial GFs over the transform-domain angular axis θ may be expressed as a sum of terms characterized in the following form, factored by a coefficient independent of $\boldsymbol{x}$,

$$\int \frac{1}{(k_i x_i + c)^n} d\theta, \tag{36}$$

with $n = 1$ for displacement, $n = 2$ for displacement gradient (equivalently, strain) and stress, and $n = 3$ for derivatives of stress. Both $\boldsymbol{k}$ and c are independent of $\boldsymbol{x}$.

The line integrals of expression (36) over a straight line between $\boldsymbol{x}^{(1)}$ and $\boldsymbol{x}^{(2)}$, as shown in Fig. 2(a), can be derived as

$$\iint \frac{1}{k_i x_i + c} d\theta dl(\mathbf{x}) = L \int \frac{\ln(k_i x_i^{(2)} + c) - \ln(k_i x_i^{(1)} + c)}{k_i x_i^{(2)} - k_i x_i^{(1)}} d\theta, \tag{37}$$

$$\iint \frac{1}{(k_i x_i + c)^2} d\theta dl(\mathbf{x}) = L \int \frac{1}{(k_i x_i^{(1)} + c)(k_i x_i^{(2)} + c)} d\theta, \tag{38}$$

$$\iint \frac{1}{(k_i x_i + c)^3} d\theta dl(\mathbf{x}) = L \int \frac{(k_i x_i^{(1)} + c) + (k_i x_i^{(2)} + c)}{2(k_i x_i^{(1)} + c)^2 (k_i x_i^{(2)} + c)^2} d\theta. \tag{39}$$

The surface integrals of expression (36) over a flat, triangular surface element with corners $\boldsymbol{x}^{(1)}$, $\boldsymbol{x}^{(2)}$ and $\boldsymbol{x}^{(3)}$, as shown in Fig. 2(b), can be derived as

$$\begin{aligned} &\iint \frac{1}{k_i x_i + c} d\theta dS(\mathbf{x}) \\ &= 2A \int \left\{ \frac{(k_i x_i^{(1)} + c)[\ln(k_i x_i^{(1)} + c) - 1]}{[k_i x_i^{(1)} - k_i x_i^{(2)}][k_i x_i^{(1)} - k_i x_i^{(3)}]} \right. \\ &+ \frac{(k_i x_i^{(2)} + c)[\ln(k_i x_i^{(2)} + c) - 1]}{[k_i x_i^{(2)} - k_i x_i^{(3)}][k_i x_i^{(2)} - k_i x_i^{(1)}]} \\ &\left. + \frac{(k_i x_i^{(3)} + c)[\ln(k_i x_i^{(3)} + c) - 1]}{[k_i x_i^{(3)} - k_i x_i^{(1)}][k_i x_i^{(3)} - k_i x_i^{(2)}]} \right\} d\theta, \end{aligned} \tag{40}$$

$$\begin{aligned} &\iint \frac{1}{(k_i x_i + c)^2} d\theta dS(\mathbf{x}) \\ &= 2A \int \left\{ \frac{-\ln(k_i x_i^{(1)} + c)}{[k_i x_i^{(1)} - k_i x_i^{(2)}][k_i x_i^{(1)} - k_i x_i^{(3)}]} \right. \\ &+ \frac{-\ln(k_i x_i^{(2)} + c)}{[k_i x_i^{(2)} - k_i x_i^{(3)}][k_i x_i^{(2)} - k_i x_i^{(1)}]} \\ &\left. + \frac{-\ln(k_i x_i^{(3)} + c)}{[k_i x_i^{(3)} - k_i x_i^{(1)}][k_i x_i^{(3)} - k_i x_i^{(2)}]} \right\} d\theta, \end{aligned} \tag{41}$$

$$\begin{aligned} &\iint \frac{1}{(k_i x_i + c)^3} d\theta dS(\mathbf{x}) \\ &= A \int \frac{1}{(k_i x_i^{(1)} + c)(k_i x_i^{(2)} + c)(k_i x_i^{(3)} + c)} d\theta. \end{aligned} \tag{42}$$

Note again that the line and surface elements should be contained in a single layer. All these integrals (34), (35) and (37)-(42) are taken in the sense of principal values in case of singularity.

It should be noted that the above expressions of physical-domain line and surface integrals of GF in multilayered solids are inapplicable in a couple of special cases. First, if the entire (field) line or surface element resides in an interface and if the source point $\boldsymbol{X}$ resides in the same interface, the transform-domain GFs are singular in various orders and a finite term must be added to the above expressions; see Pan and Yang (2003) for detail in the case of the so-called interfacial GF. However, the analytical form of this finite term in the transform domain after integration over the physical domain is unclear to us. It is instead evaluated by carrying out the integration first over the transform domain and then over the physical domain. By realizing that the interfacial GF is proportional

Table 1 : Materials properties of AlN, InN and GaN in the reduced notation (elastic constant C_{ij} in GPa, piezoelectric constants e_{ij} in C/m^2, and dielectric constants ε_{ij} equal to ε_{ijr} x 8.854 x 10^{-12} C/(V·m)). The other nonzero components include C_{22} (= C_{11}),C_{23} (= C_{13}),C_{55} (= C_{44}), C_{66} (= ($C_{11} - C_{12}$)/2), e_{32} (= e_{31}), e_{24} (= e_{15}), and ε_{22} (= ε_{11}).

Material	C_{11}	C_{12}	C_{13}	C_{33}	C_{44}	e_{31}	e_{33}	e_{15}	ε_{11r}	ε_{33r}
AlN	410	149	99	389	125	–0.58	1.55	–0.48	8.5	8.5
InN	190	104	121	182	10	–0.57	0.97	–0.22	15.3	15.3
GaN	390	145	106	398	105	–0.33	0.65	–0.30	8.9	8.9

to r^{-n} (where n is a known integer, and r is the distance between field and source points) and is thus virtually a 1D function in terms of η (where η is the angle between the position vector from the source point to the field point and a reference line within the interface), its physical-domain integrals can be obtained semi-analytically and efficiently. The other case, which is similar to the first one, is a (triangular) surface element with (only) one edge residing in an interface and the source point $\boldsymbol{X}$ residing in the same interface. It is however much more troublesome than the first case. It is as yet unclear to us how the corresponding finite term could be added efficiently. This problem may be solved by lifting the edge touching an interface a little away from the interface so that the finite term can be attained numerically. The tradeoff is that the resulting integral is near-singular.

4 Numerical Examples

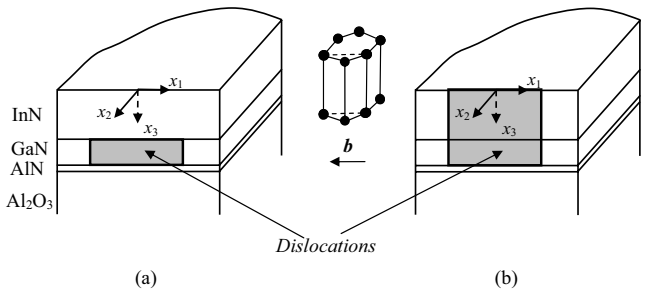

Figure 3 : (a) A closed-loop dislocation and (b) a half-loop dislocation in a multilayered heterostructure of InN/GaN/AlN on a semi-infinite Al_2O_3 substrate.

In this section, we apply the previous formulation to calculate the elastic and electric fields produced by a dislocation in multilayered InN/GaN/AlN over a semi-infinite Al_2O_3 substrate, as schematically shown in Fig. 3. The material system was experimentally studied by Lu et al. (2003). In our simulation, the finite layers are taken to have thickness of 760 nm for InN, 245 nm for GaN, and 14 nm for AlN. All these materials except Al_2O_3 are assumed to exhibit the piezoelectric coupling effect. The InN, GaN and AlN materials are taken to have the wurtzite structure and thus are transversely isotropic, while the Al_2O_3 material is assumed to be isotropic. The isotropy axis of InN, GaN and InN, which is also the poling axis, is taken to be normal to the top surface and interfaces. Their elastic, electrical and piezoelectric constants are given in Table 1 (Levinshtein et al., 2001). In addition, Young's modulus = 300 GPa, Poisson's ratio = 0.22, and dielectric constant ε = 9 x 8.854 x 10^{-12} C/(V·m) for Al_2O_3.

A detailed discussion of the possible dislocation systems in wurtzite crystals can be found in the text by Hirth and Lothe (1991). In our simulation, a $(11\bar{2}0)$ dislocation is considered. Its slip plane is vertical, taken to be normal to the x_2 axis. The Burgers vector $\boldsymbol{b}$ is along the x_1 axis. Two cases of a dislocation are analyzed. First, a (rectangular) closed-loop dislocation is considered, as shown in Fig. 3(a). It vertically spans the GaN layer. Thus, it consists of two interfacial line dislocation segments (of screw type) and two vertical threading dislocation segments (of edge type), in the conventional terminology of *line* dislocations (Hirth and Lothe, 1991). The second case is a half-loop dislocation, located in the top two layers, and extending to the top surface, as shown in Fig. 3(b). This defect system consists of an interfacial line dislocation segment (of screw type) at the interface between GaN and AlN layers, and two threading dislocation segments (of edge type) extending from the interface between GaN and AlN layers to the top surface. In addition, it consists of an interfacial step at the InN and GaN interface, and a surface step on the top surface. Results of the two cases are presented below. In the results, the thickness of the GaN layer, l_0 = 245 nm, is used to nor-

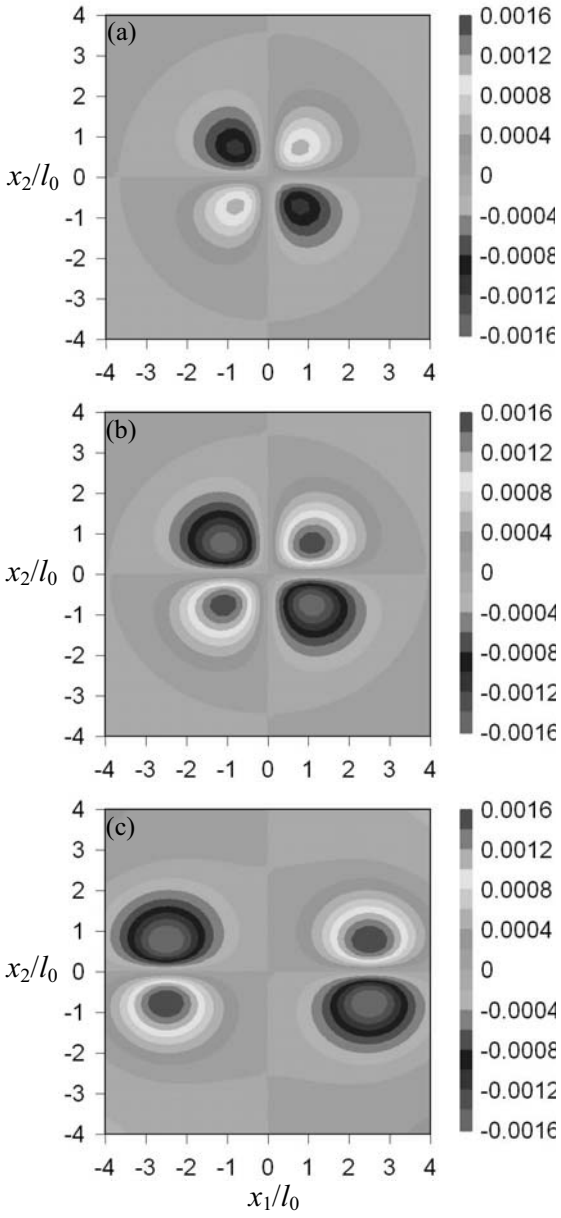

Figure 4 : Contour plots of normalized hydrostatic strain field $\gamma_{kk} l_0/b$ on the top surface due to a closed dislocation loop (Fig. 3(a)) at various lateral span widths (a) 1 l_0; (b) 2 l_0 and (c) 5 l_0.

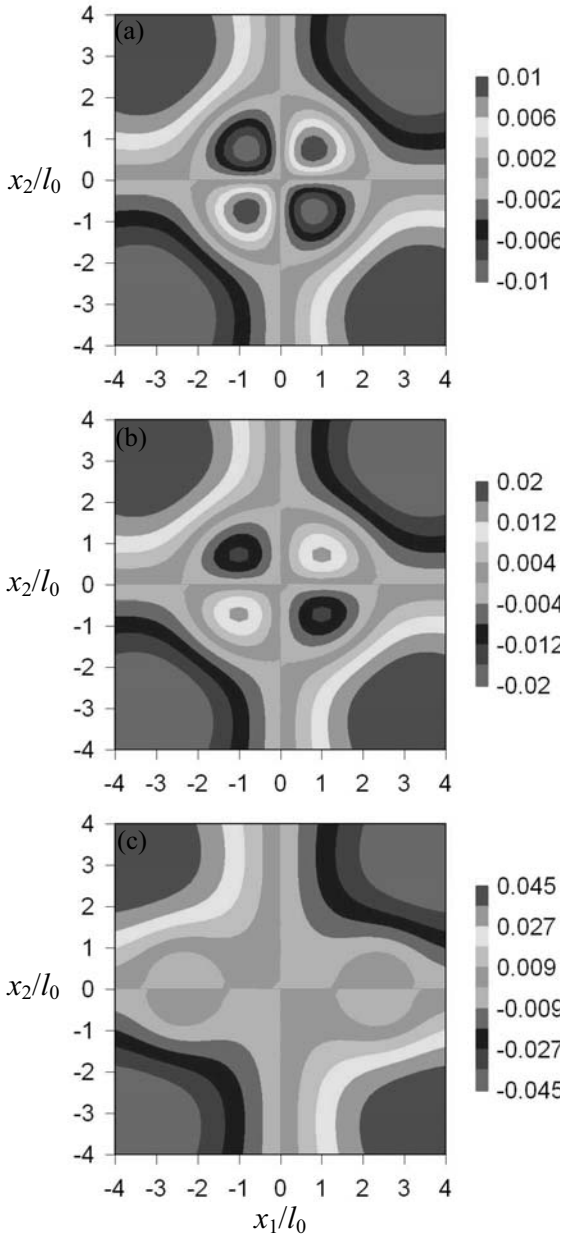

Figure 5 : Contour plots of normalized electrical potential field $\theta/(E_0 b)$ on the top surface due to a closed-loop dislocation (Fig. 3(a)) at various lateral span widths (a) 1 l_0; (b) 2 l_0 and (c) 5 l_0.

malize all quantities of the dimension of length. E_0 = 1 GV/m is used to normalize all quantities of the dimension of electrical field. Since the problem is linear, the induced fields are all scaled by the normalized Burgers vector, b/l_0.

In the first case of a closed-loop dislocation, the induced fields of hydrostatic strain γ_{kk} ($=\gamma_{11}+\gamma_{22}+\gamma_{33}$) and electric potential ϕ on the top surface are examined. The results are plotted in contour for three values of dislocation lateral span width, equal to 1 l_0, 2 l_0, and 5 l_0, in Figs. 4(a-c) and 5(a-c). These figures show that when the dislocation lateral span increases, i.e., when the two opposite threading dislocations move away from each other, each field is split into two disassociated, localized spots. This

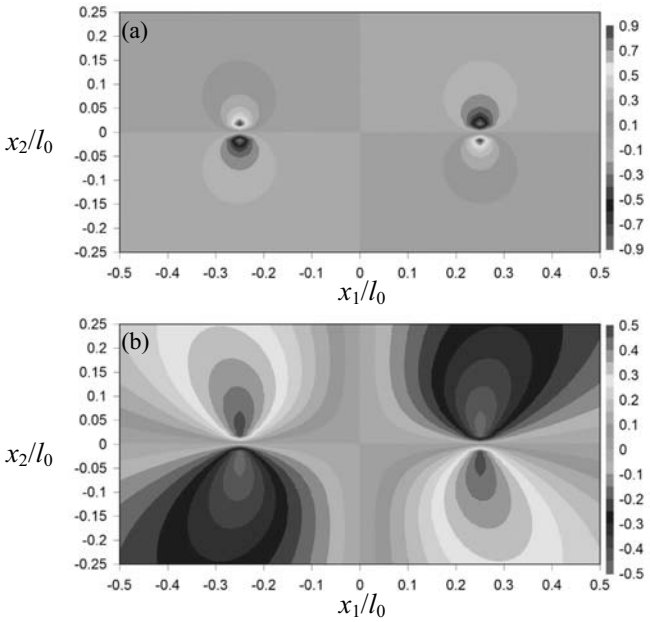

Figure 6 : Contour plots of (a) normalized hydrostatic strain field $\gamma_{kk} l_0/b$ and (b) electrical potential field $\theta/(E_0 b)$ on the top surface due to a half-loop dislocation (Fig. 3(b)) with lateral width equal to 0.5 l_0.

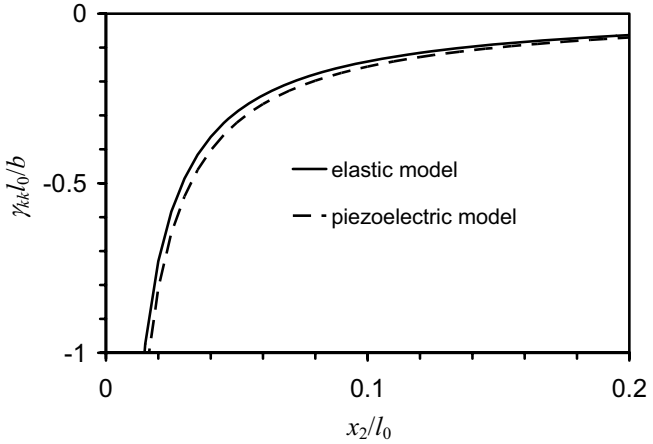

Figure 7 : Variation of normalized hydrostatic strain $\gamma_{kk} l_0/b$ along a straight line (x_1=0.25 l_0, x_2, x_3=0) on the top surface due to a half-loop dislocation (Fig. 3(b)) with lateral span width equal to 0.5 l_0.

means that the two interfacial screw dislocations do not induce any field on the top surface–only the two threading edge dislocations do. Both γ_{kk} and ϕ on the top surface are anti-symmetric. This explains why the total field decreases when the two threading dislocations approach each other. It was also checked that the induced stress field satisfies the traction-free boundary condition on the top surface. The normal component of induced electrical displacement is equal to zero as well, which is a part of the boundary condition as enforced in the GF used to compute the fields due to a dislocation.

In the second case of a half-loop dislocation, the induced fields of hydrostatic strain γ_{kk} and electric potential ϕ on the top surface are calculated with dislocation lateral span width equal to 0.5 l_0. The surface and interfacial steps are not accounted for. The nature of the surface step is unclear to us. The interfacial step is modeled as a line-force defect, with force density estimated as described before. However, although the lattice-constant mismatch is 10 %, it turns out that the effect of the interfacial step is insignificant compared to that of the dislocation when the observation point is on the top surface. The fields due to the dislocation alone are plotted in contour in Figs. 6(a) and (b). Since the threading dislocations terminate at the top surface, the induced fields around them are singular. For comparison, the material system is modeled as completely elastic in order to show how significant the piezoelectric coupling effect is on the induced strain field. The field is evaluated along a line (x_1=0.25 l_0, x_2, x_3=0) on the top surface, which originates at one threading dislocation tip, and extends along the x_2 axis. The fields of γ_{kk} due to the elastic and piezoelectric models are plotted for comparison in Fig. 7. A slight contribution of the piezoelectric coupling effect to the induced strain field can be seen. The variation was also plotted on a logarithmic scale. This shows that the order of singularity is r^{-1} in the strain field in the vicinity of the threading dislocation tip on the top surface, predicted by both the elastic and piezoelectric models, consistent with the previous understanding about a line dislocation (Mura, 1982). However, this variation by r^{-1} holds only for a finite distance, showing the effect of the other threading dislocation as well as that of the interfaces.

5 Conclusions

An efficient scheme has been developed for evaluation of the physical-domain line and surface integrals of a GF in multilayered generally anisotropic and linearly piezoelectric (including elastic as a special case) materials. The line and surface integrals of a GF are required in the modeling of line and surface defects such as steps

and dislocations. The high efficiency in evaluation of the integrals is achieved by analytically carrying out the integration over the physical domain. This enabels us to efficiently simulate a relatively large system of various defects, including line and surface defects as well as point defects in a complex heterogeneous material system. The highly efficient evaluation of surface integral of the GF is particularly valuable to the moldeing of dislocations due to the lack of a line-defect treatment of this group of defects, which are originally modeled as a uniform planar distribution of force dipoles, in a multilayered heterogeneous matrix. Numerical simulations of dislocations in a realistic nanostructure of multilayered InN/GaN/AlN on a semi-infinite Al_2O_3 substrate are presented to demonstrate the efficiency and accuracy of the present scheme.

References

Arias, R. and Lund, F. (1999): Elastic fields of stationary and moving dislocations in three-dimensional finite examples, *Journal of the Mechanics and Physics of Solids*, vol. 47, 817-841.

Balamane, H., Halicioglu, T., and Tiller, W. A. (1992). Comparative study of silicon empirical interatomic potentials, *Physical Review B* vol. 46, 2250-2279.

Barnett, D.M. and Lothe, J. (1975): Dislocations and line charges in anisotropic piezoelectric insulators, *Physica Status Solidi B* vol. 67, 105-111.

Eshelby, J. D. (1956): The continuum theory of lattice defects, in *Solid State Physics: Advances in Research and Applications*, ed. F. Seitz and D. Turnbull, Academic Press Inc., Publishers, New York.

Ghoniem, N. M. and Han, X. (2005): Dislocation motion in anisotropic multilayer materials, *Philosophical Magazine* vol. 85, 2809-2830.

Gosling, T. J. and Willis, J. R. (1994): A line-integral representation for the stresses due to an arbitrary dislocation in an isotropic half-space, *Journal of the Mechanics and Physics of Solids* vol. 42, 1199-1221.

Han, X. and Ghoniem, N. M. (2005): Stress field and interaction forces of dislocations in anisotropic multilayer thin films, *Philosophical Magazine* vol. 85, 1205-1225.

Heying, B., Tarsa, E. J., Elsass, C. R., Fini, P., DenBaaes, S. P. and Speck, J. S. (1999): Dislocation mediated surface morphology of GaN, *Journal of Applied Physics* vol. 85, 6470-6476.

Hill, R. (1961): Discontinuity relations in mechanics of solids, in *Progress in Solid Mechanics 2*, ed. I. Sneddon and R. Hill, North-Holland, Amsterdam, 247-276.

Hirth, J. P. and Lothe, J. (1991): *Theory of Dislocations*, 2^{nd} ed., Krieger Publishing Company, Malabar, Florida.

Kanzaki, H. (1957): Point defects in face-centred cubic lattice-I distortion around defects, *Journal of Physics and Chemistry of Solids* vol. 2, 24-36.

Levinshtein, M. E., Rumyantsev, S. L. and Shur, M. (2001): *Properties of Advanced Semiconductor Materials (GaN, AlN, InN, BN, SiC, SiGe)*, John Wiley & Sons, Inc.

Liu, F., Tersoff, J. and Lagally, M. G. (1997): Self-organizatopm of steps in growth of strained films on vicinal substrates, *Physical Review Letters* vol. 80, 1268-1271.

Look, D. C. and Sizelove, J. R. (1999): Dislocation scattering in GaN, *Physical Review Letters* vol. 82, 1237-1240.

Love, A. E. H. (1944): *A Treatise on the Mathematical Theory of Elasticity*, Dover.

Lu, C. J., Bendersky, L. A., Lu, H. and William, J. S. (2003): Threading dislocations in epitaxial InN thin film grown on (0001) sapphire with a GaN buffer layer, *Applied Physics Letters* vol. 83, 2817-2819.

Maradudin, A. A., Montroll, E. W., Weiss, G. H., and IPaTova, I. P. (1971): *Theory of Lattice Dynamics in the Harmonic Approximation*, Academic Press.

Mura, T. (1963): Continuous distribution of moving dislocations, *Philosophical Magazine* vol. 8, 843-857.

Mura, T. (1982): *Micromechanics of Defects in Solids*, Martinus Nijhoff Publishers, Boston.

Nemat-Nasser, S. and Hori, M. (1999): *Micromechanics: Overall Properties of Heterogeneous Materials*, 2^{nd} ed., Elsevier Science, Netherlands.

O'Day, M. P. and Curtin, W. A. (2004): A superposition framework for discrete dislocation plasticity, *Journal of Applied Mechanics* vol. 71, 805-815.

Pan, E. and Tonon, F. (2000): Three-dimensional Green's functions in anisotropic piezoelectric solids, *International Journal of Solids and Structures* vol. 37, 943-958.

Pan, E. and Yuan, F. G. (2000a): Three-dimensional Green's functions in anisotropic bimaterials, *International Journal of Solids and Structures* vol. 37, 5329-5351.

Pan, E. and Yuan, F. G. (2000b): Three-dimensional Green's functions in anisotropic piezoelectric bimaterials, *International Journal of Engineering Science*, vol. 38, 1939-1960.

Pan, E. and Yang, B. (2003): Three-dimensional interfacial Green's functions in anisotropic bimaterials. *Appllied Mathematical Modelling* vol. 27, 307-326.

Stroh, A. N. (1958): Dislocations and cracks in anisotropic elasticity, *Philosophical Magazine* vol. 3, 625-646.

Swamy, K., Bertel, E. and Vilfan, I. (1999): Step interaction and relaxation at steps: Pt(110), *Surface Science* vol. 425, L369-L375.

Tewary, V. K. (1973): Green-function method for lattice statics, *Advances in Physics* vol. 22, 757-810.

Tewary, V. K. (2004): Multiscale Green's-function method for modeling point defects and extended defects in anisotropic solids: Application to a vacancy and free surface in copper, *Physical Review B* vol. 69, 094109-1-13.

Tewary, V. K. and Read, D. T. (2004): Integrated Green's function molecular dynamics method for multiscale modeling of nanostructures: Application to Au nanoisland in Cu, *CMES: Computer Modeling in Engineering & Science* vol. 6, 359-371.

Ting, T. C. T. (1996): *Anisotropic Elasticity*, Oxford University Press, Oxford.

Van de Walle, C. G., Stampfl, C. and Neugebauer, J. (1998): Theory of doping and defects in III-V nitrides, *Journal of Crystal Growth* vol. 189/190, 505-511.

Wang, C. Y. (1997): Elastic fields produced by a point source in solids of general anisotropy, *Journal of Engineering Mathematics* vol. 32, 41-52.

Weygand, D., Friedman, L. H., Van der Giessen, E. and Needleman, A. (2002): Aspects of boundary-value problem solutions with three-dimensional dislocation dynamics, *Modeling and Simulation in Materials Science and Engineering* vol. 10, 437-468.

Yang, B. and Pan, E. (2002a): Three-dimensional Green's functions in anisotropic trimaterials, *International Journal of Solids and Structures* vol. 39, 2235-2255.

Yang, B. and Pan, E. (2002b): Efficient evaluation of three-dimensional Green's functions in anisotropic elastostatic multilayered composites, *Engineering Analysis with Boundary Elements* vol. 26, 355-366.

Yang, B., Pan, E. and Tewary, V. K. (2004): Static responses of a multilayered anisotropic piezoelectric structure to point force and point charge, *Smart Materials and Structures* vol. 13, 175-183.

Yang, B. and Tewary, V. K. (2005): Green's function-based multiscale modeling of defects in a semi-infinite silicon substrate, *International Journal of Solids and Structures* vol. 42, 4722-4737.

Yu, H. Y. and Sanday, S. C. (1993): Elastic fields due to centers of dilatation and thermal inhomogeneities in plane-layered solids, *Journal of the Mechanics and Physics in Solids* vol. 41, 267-296.

Yuan, F. G., Yang S. and Yang, B. (2003): Three-dimensional Green's functions for composite laminates, *International Journal of Solids and Structures* vol. 40, 331-342.